sustainability

MDPI

Article

High-Performance Flywheel Hybrid Powertrain

Hong Li [1], Jiangwei Chu [1,*] and Shufa Sun [2]

[1] School of Traffic and Transportation, Northeast Forestry University, Harbin 150040, China; lihong9012@nefu.edu.cn
[2] College of Engineering and Technology, Northeast Forestry University, Harbin 150040, China; ssfangel@nefu.edu.cn
* Correspondence: cjw_62@nefu.edu.cn

Abstract: The high efficiency of the flywheel hybrid powertrain, as well as its power characteristics, can help to meet high energy/power conversion needs, which may prove to be promising. Moreover, the flywheel hybrid powertrain may reduce dependence on batteries. This paper presents the EC-BERS in order to capture more mechanical power than its rated power, and to reduce the charge/discharge cycles of the battery. In this new energy recovery system, maximum torque can be obtained in the higher speed zone, leading to two marked improvements in terms of improving the braking efficiency. The working point of the system changes and shifts to the high-speed zone to meet the maximum torque at higher speeds. Furthermore, this powertrain can transfer the vehicle kinetic energy into the flywheel directly in the same form. Only the slip energy needs to be dealt with in the electrical form, which is beneficial to prolonging the battery life. Two typical systems were emulated under the same conditions to verify this feature, and a small prototype was designed to prove the concept.

Keywords: hybrid powertrain; flywheel; energy recovery; power characteristic

check for updates

Citation: Li, H.; Chu, J.; Sun, S. High-Performance Flywheel Hybrid Powertrain. *Sustainability* **2022**, *14*, 8076. https://doi.org/10.3390/su14138076

Academic Editors: Eric Cheng and Junfeng Liu

Received: 10 June 2022
Accepted: 29 June 2022
Published: 1 July 2022

Publisher's Note: MDPI stays neutral with regard to jurisdictional claims in published maps and institutional affiliations.

Copyright: © 2022 by the authors. Licensee MDPI, Basel, Switzerland. This article is an open access article distributed under the terms and conditions of the Creative Commons Attribution (CC BY) license (https://creativecommons.org/licenses/by/4.0/).

1. Introduction

Climate change is a current global issue, and its impact is huge. Since the first industrial revolution, human beings have emitted more than 1.48 trillion tons of carbon dioxide into the atmosphere by burning fossil fuels [1,2]. In 2021, the IPCC released its climate change report, which stated that the world is likely to temporarily warm by 1.5 C over the next 20 years, even if greenhouse gas emissions are drastically reduced [3]. Figure 1 shows the CO_2 emissions of major carbon emitting countries in North America, the Middle East and the Asia–Pacific region from 2009 to 2019 [4]. The absolute carbon emissions of large economies such as the United States, China and India account for about 50% of the world's emissions. In this context, all countries in the world agreed to reduce greenhouse gas emissions. China has put forward the "carbon peak and carbon neutrality" goal, which aims to peak carbon emissions before 2030 and achieve carbon neutrality by 2060 [5]. At present, more than 120 countries have formulated targets and measures in relation to "carbon peak and carbon neutrality" [6].

According to some statistics, transportation accounts for the third largest share of energy consumption in the world and is growing fastest [7]. On 27 October 2020, the "Energy-saving and New-Energy Vehicle Technology Roadmap 2.0", published at the annual meeting of the Society of China SAE, pointed out that the revolution of energy, interconnection and intelligence had injected strong new impetus into the innovation and development of the automobile industry. The average fuel consumption of a new-energy vehicle in China has been continuously decreasing and is approaching the target value of 5 L/100 km (2020) [8]. The overall goal of China's automobile development is that, in the next 10–15 years, total carbon emissions will be ahead of the national carbon emission reduction commitment, peak in 2028, and in 2035 the total carbon emissions will reduce

by 20% from the peak. The automobile industry has presented a situation that several technological routes in low-carbon are developing in parallel, and the reduction of carbon emissions in the automobile industry is of profound significance to the ultimate goal of global carbon neutrality.

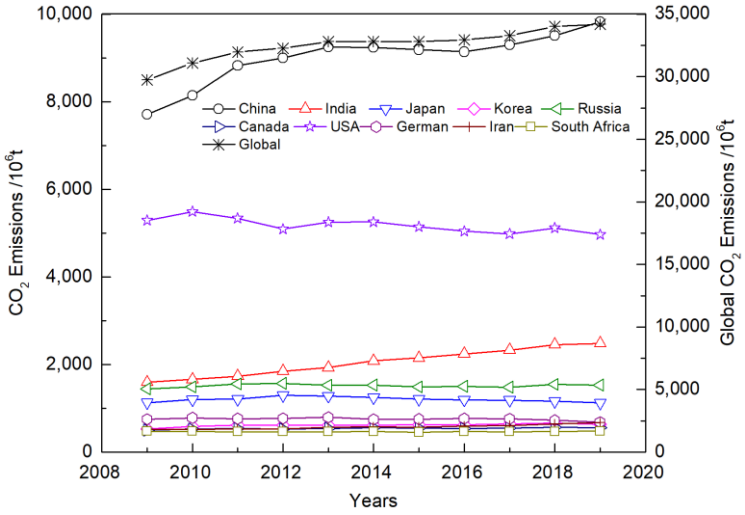


Figure 1. CO_2 emissions in some countries (2009–2019) [4].

Regenerative braking technology in motors plays a key role in fuel saving in EVs/HEVs. For example, a Toyota Prius equipped with a full hybrid system has achieved braking energy recovery. However, the output power is limited by the Ni–MH battery which results in a recovered brake energy of less than 30 kW, and the total motor capacity (about 100 kW) in the power train cannot be fully utilized. Moreover, its performance with the power assistant is also limited by the battery's poor output power [9]. Under ideal conditions, if the vehicle can recover all kinetic energy during braking, its powertrain system only needs to provide the power to overcome friction losses, such as air resistance, road resistance, and other mechanical friction [10–12]. As the mainstream braking technology in hybrid electric vehicles, motor regenerative braking technology can transform part of a vehicle's kinetic energy into electrochemical energy, but there are many factors affecting the energy utilization efficiency in this process [13–16]. Among them, the power of the electric drive system becomes the biggest factor restricting the recovery efficiency, which cannot provide greater mechanical power than its rated power [17–19]. If the braking power requirement exceeds the powertrain rating, the ECU will activate the hydraulic braking system to meet the braking requirement. Therefore, it is important to improve the energy recovery efficiency while protecting the cycle life of the batteries.

Energy storage devices for the EV/HEV should meet the power and energy requirements under different driving conditions. Batteries, as the primary source for electric vehicles, cannot offer high energy density, high power density and low cost at the same time [20,21]. They are better at the required high energy capabilities. Ultracapacitors are preferred for applications where high-peak current and power is required [22]. The main characteristics of the ultracapacitors mentioned above can also be applied to flywheels. The difference between them is in the discharge pulse size and available energy [23]. The motor regenerative braking technology is capable of transferring energy from mechanical energy to electrochemical energy and vice versa [24,25]. However, it should be noted that there was efficiency loss in the energy conversion process. Especially when the braking time is short, the energy storage speed is restricted by the chemical reaction speed of the battery electrode "active substance", and the energy recovery efficiency is lower. In order to solve the shortcomings of the battery, ultracapacitors could achieve high efficiency and superior power control in a short time, especially suitable for unpredictable urban conditions. However, this paper introduces a flywheel hybrid power system from another perspective

to capture/release high power [26,27]. Among the several typical energy storage devices, flywheel energy storage possesses the characteristics of high instantaneous power and fast response, making it one of the energy storage technologies with a promising future [28–31]. Therefore, a new approach of storing a vehicle's kinetic energy by flywheel, the electromagnetic coupling braking energy recovery system (EC-BERS), was proposed, which can transfer most of the kinetic energy in the deceleration process into the flywheel's kinetic energy directly, making it possible to capture more power than rated power. At the same time, the battery processes less energy, which is beneficial to prolonging the battery life.

2. Brake Energy Recovery System

2.1. Two-Scenario Structure

The PMSM-based BERS is shown in Figure 2a, wherein the permanent magnet synchronous motor (PMSM) is connected with the differential mechanically through the first gear pair. The structure of the EC-BERS is shown in Figure 2b, wherein the electromagnetic couplers replace the permanent magnet synchronous motor and are arranged between the flywheel and wheel. A more detailed description can be found in Section 3.1. When the vehicle decelerates, the wheel drives the flywheel to rotate after increasing by half shaft, differential, first-stage gear, electromagnetic coupler and second-stage gear, storing partial kinetic energy in the flywheel directly.

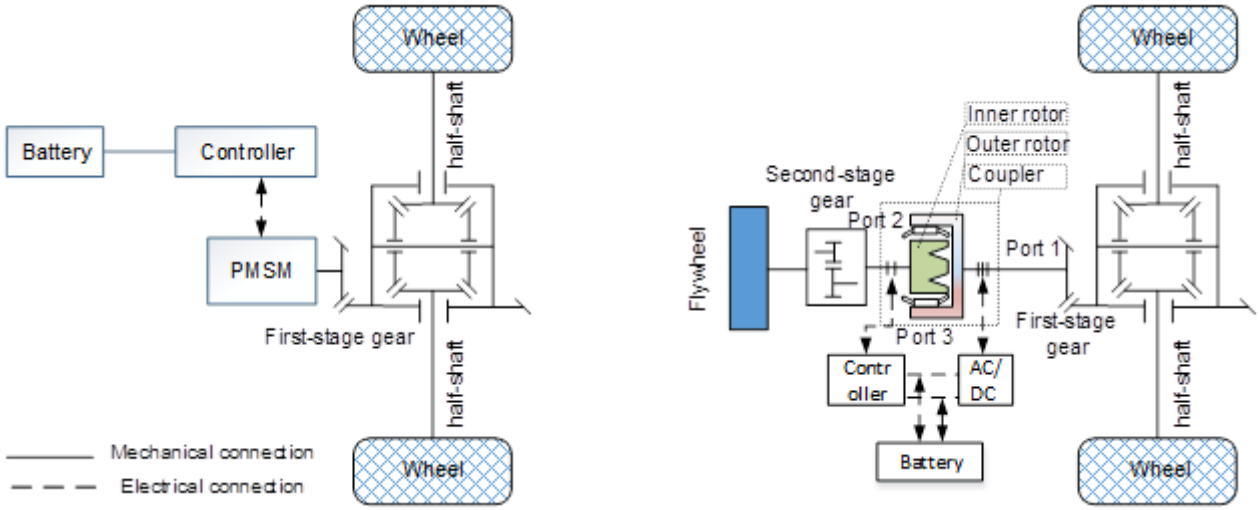


Figure 2. Structure of braking energy recovery system: (**a**) PMSM-based BERS; (**b**) EC-BERS.

2.2. Powertrain Power Flow

In order to describe the energy transfer of the system quantitatively, it is assumed that the active power from or transmitted to the outer rotor shaft is P_o, and the electromagnetic power, iron-loss, mechanical power, slip power, mechanical-loss, electric machine-losses and battery-losses are P_{me}, P_{Fe}, P_{mech}, P_s, P_{ml}, P_{el} and P_{bl} [32], respectively. The active power from or transmitted to the inner rotor shaft is P_i. For the EC-BERS, the vehicle operating states include start-up, acceleration, cruise, deceleration and stop. In order to highlight the power–torque–speed characteristics of the proposed system, this section mainly demonstrates the power-flow under the deceleration and acceleration states. In fact, the flywheel's speed can be zero at start-up if the vehicle is stationary for a long time. However, if the vehicle slows to a stop for a short time, the initial speed of the flywheel on the next start may not be zero, due to the previous kinetic energy capture. In Section 4.2, the initial state of the flywheel conforms to the second case, with a speed of 4395 rpm. When the vehicle stops, the outer rotor is at rest. At this time, if the flywheel rotates, the electromagnetic coupler acts as a generator, and current will be induced in the outer rotor winding to charge the battery through AC/DC.

In the deceleration state, part of the vehicle kinetic energy is stored in the flywheel through the two-gear pairs. Figure 3a shows the flywheel energy storage device and represents the energy conversion process in which the outer rotor angular velocity is greater than the inner rotor. The mechanical power (P_i) is stored in the flywheel through the second-stage gear, and the magnetic power (P_e) is stored in the battery. Assuming a situation where the angular velocity of the outer rotor is about same as the inner rotor, the slip power is approximately zero, as shown in Figure 3b.

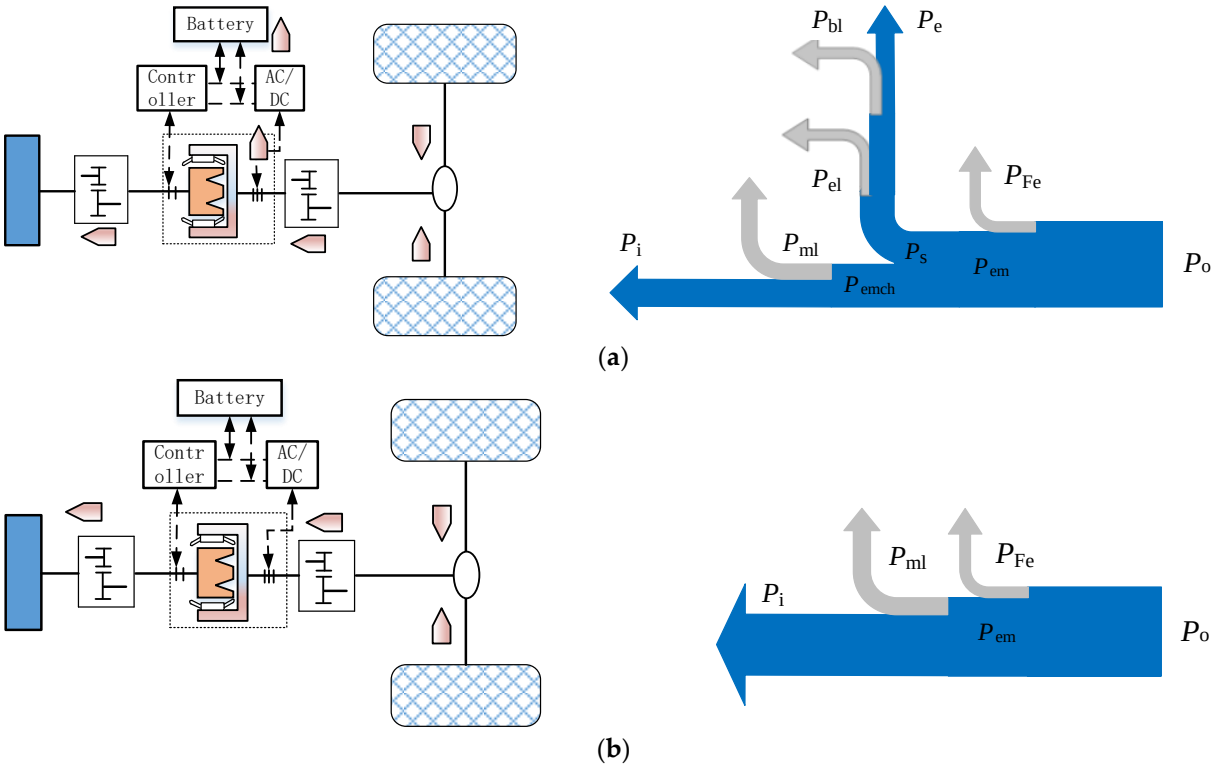


Figure 3. Energy conversion process under deceleration conditions: (**a**) $\omega_o > \omega_i$; (**b**) $\omega_o = \omega_i$.

Under the acceleration state, the energy stored in the flywheel releases on the rear wheel. Figure 4a represents the energy conversion process in which the angular velocity of the inner rotor is greater than the outer rotor. The mechanical power of the electromagnetic coupler acts on the rear wheel after the first-stage gear decelerates, and the power Pe is stored in the battery via the AC/DC. Figure 4b shows the energy conversion process when $\omega_o = \omega_i$.

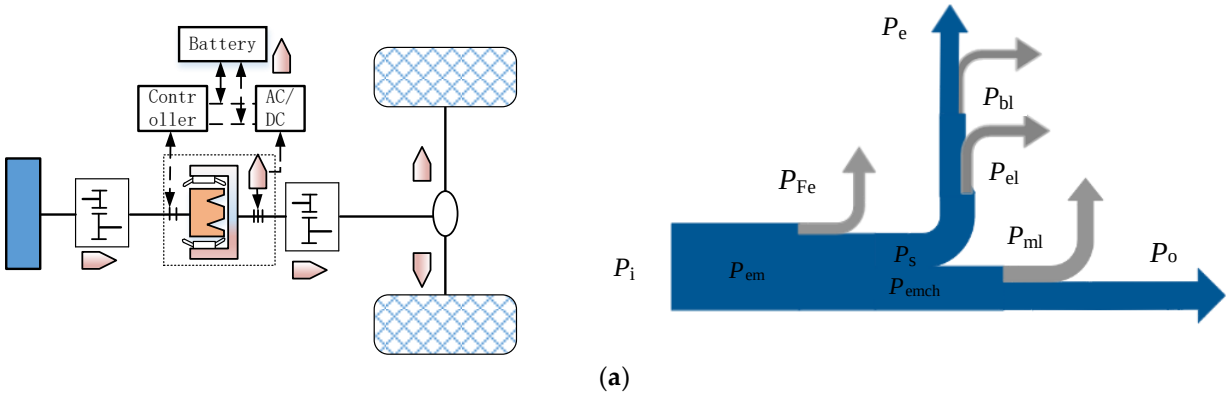


Figure 4. *Cont.*

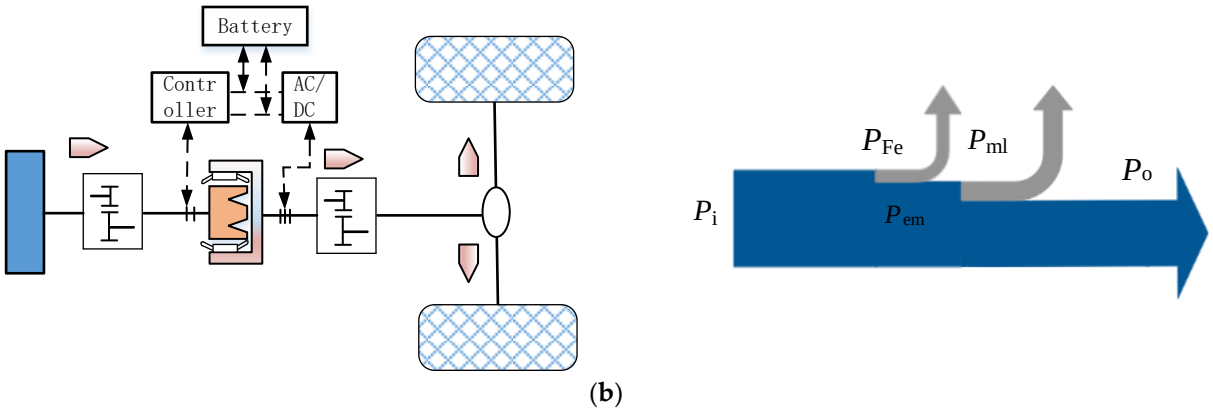


Figure 4. Energy conversion process under acceleration conditions: (**a**) $\omega_o < \omega_i$; (**b**) $\omega_o = \omega_i$.

3. Powertrain Modeling

3.1. Electromagnetic Coupler Overview

The electromagnetic coupler is a dual mechanical port motor, wherein the electrical port is connected to the battery through the converter, the outer rotor is connected to the rear wheel, and the inner rotor is connected to the flywheel, as shown in Figure 2b. Therefore, kinetic energy can be directly transferred from one mechanical port to another [33–37]. It follows the same electromagnetic rules as a normal motor. The amplitudes of torque produced on port 1 and port 2 are same. As long as there is relative movement between the mechanical ports, the magnetic flux of the rotor will change repeatedly, inducing currents in the outer rotor windings. Meanwhile, the amount of power transmitted through the mechanical port is determined by the electrical port. If the inner rotor is fixed, the electromagnetic coupler is an ordinary motor and its mathematical model in the dq coordinate system is as follows. Physical quantity name and symbol is given in Abbreviations.

$$\begin{cases} u_{oq} = R_r i_{oq} + \dot{\psi}_{oq} + p(\omega_o - \omega_i)\psi_{od} \\ u_{od} = R_r i_{od} + \dot{\psi}_{od} - p(\omega_o - \omega_i)\psi_{oq} \\ \psi_{od} = L_m i_f + L_{od} i_{od} \\ \psi_{oq} = L_{oq} i_{oq} \\ T_e = 1.5p(\psi_{od} i_{oq} - \psi_{oq} i_{od}) \end{cases} \tag{1}$$

$$\begin{cases} T_{mo} = J_o \frac{d\omega_o}{dt} + B_o \omega_o + T_{eo} \\ T_{mi} = J_i \frac{d\omega_i}{dt} + B_i \omega_i + T_{ei} \\ T_{eo} = -T_{ei} = 1.5p\left[(L_{od} - L_{oq}) i_{oq} i_{od} - L_m i_f i_{oq}\right] \\ T_{eo} = T_{ei} = T_e \end{cases} \tag{2}$$

3.2. Power Characteristics

In order to describe the power characteristics of the EC-BERS quantitatively, the slip angular velocity and slip power are defined as $\Delta\omega$, P_s. The angular velocity, power and torque of the electromagnetic coupler at rated state are ω_N, P_N and T_N. The relationship between variables satisfies the following equation:

$$\begin{cases} \Delta\omega = \omega_o - \omega_i \\ P_N = T_N \omega_N \end{cases} \tag{3}$$

It is assumed that the electromagnetic coupler works at the rated torque and meets $\omega_i = i\,\omega_N$, $\omega_o = (i + 1)\,\omega_N$ and $i \geq 0$. The power of the inner and outer rotor, slip power and slip angular velocity of the coupler is as follows:

$$\begin{cases} P_o = (i+1)T_N\omega_N \\ P_i = iT_N\omega_N \\ P_s = |P_o - P_i| = P_N \\ \Delta\omega = |\omega_o - \omega_i| = \omega_N \end{cases} \quad (4)$$

Table 1 shows the power, torque and speed of the mechanical ports of the electromagnetic coupler when i = 0, 1.0 and 1.5. When i = 0, it means the inner rotor is fixed, and the electromagnetic coupler is equivalent to an ordinary motor. The T-ω and P-ω curves are shown as the purple area in Figure 5. When i > 0, the inner rotor is unfixed, and the electromagnetic coupler is equivalent to a double-mechanical motor. Due to the rotation of the inner rotor shaft, the induced voltage on the winding is reduced, and the torque–speed characteristics of the coupler move right, where i = 1.0 corresponds to the blue region, and i = 1.5 corresponds to the yellow region, as shown in Figure 5.

Table 1. Power transfer characteristics of mechanical ports of electromagnetic coupler.

Operative State	i	ω_i	ω_o	P_i	P_o
The inner rotor is fixed	0	0	ω_N	0	P_N
The inner rotor is removed from fixation	1.0	ω_N	2 ω_N	P_N	2.0 P_N
	1.5	1.5 ω_N	2.5 ω_N	1.5 P_N	2.5 P_N

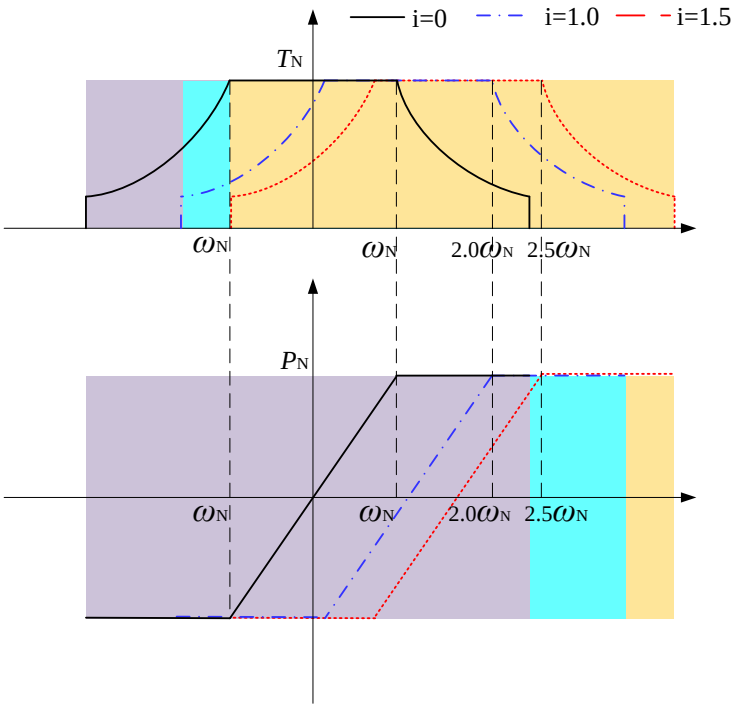


Figure 5. Electrical port characteristics of electromagnetic coupler.

Although the traditional electric drive system has good acceleration performance at low speed, it has the problem of insufficient driving torque because it works in a constant power region at high speed. On the other hand, when traditional electric vehicles brake at high speed, the regenerative braking force of the motor is limited by the available output torque of the motor. It can be seen from the T-ω characteristics in Figure 5 that the electromagnetic coupling braking energy recovery system can give full play to the

maximum torque under different speed ranges, that is, the working point of the system changes and moves to the high-speed zone. According to Formula (4), assuming that the EC-BERS operates at rated torque, the power transferred by the mechanical ports is much greater than its rated power. The flywheel recovery power from the wheels is not limited by the motor rated power, and the energy is stored in the form of mechanical energy directly. As a result, only the slip energy needs to be dealt with in electrical form and stored in the battery.

4. A Typical Case Study

The two scenarios given in Figure 2 will be discussed. In scenario one, a conventional PMSM-based BERS is used to capture braking energy. In scenario two, the EC-BERS substitutes for the PMSM-based BERS to capture the same braking deceleration rates as scenario one. In order to make the comparison more convincing, the parameters between the PMSM and the electromagnetic coupler are set as the same in Matlab/Simulink, shown in Table 2. For a typical family car, the mass of the flywheel is about 10 to 15 kg, with a diameter of about 40 cm, and its inertia is about 0.2 to 0.3 kg·m^2. With the data as reference, the inertia of the flywheel in the proposed system is set as 0.3 kg·m^2. As the composite rotor application, the flywheel can meet the requirements of kinetic energy storage with a smaller inertia (or mass). For example, a 10 kg idealized rim made of IM9/epoxy has a maximum kinetic energy of 2570 W·h, about 9.48 times that of steel 4340 [23]. Therefore, the composite rotor has great application value for the vehicle. In the process of vehicle deceleration–cruise, the PMSM and electromagnetic coupler all operate at rated torque to obtain a larger braking torque. According to the voltage equation in Formula (1), the dq components of the current are coupled. In order to realize current decoupling, the decoupling feedforward control strategy is adopted. Based on the above methods, the control block diagram of the electromagnetic coupler is established, as shown in Figure 6.

Table 2. Case study parameters.

Vehicle Parameters	Unit	Value
Mass	kg	1650
Wheel radius	m	0.316
Flywheel Parameters	Unit	Value
Inertias	kg·m^2	0.3
Maximum speed	rpm	25,000
Initial speed	rpm	4395
Mass	kg	15
Gear Pair Parameters	Unit	Value
First stage	-	1:4
Second stage	-	1:5
PMSM Parameters	Unit	Value
Rated power	kW	5.5
Rated speed	r·min^{-1}	1750
Rated torque	N·m	30.0
Battery Parameters	Unit	Value
Capacity	W·h	780
SOC	%	70
Open-circuit Voltage	V	120
Electromagnetic Coupler Parameters	Unit	Value
Rated power	kW	5.5
Rated speed	r·min^{-1}	1750
Rated torque	N·m	30.0

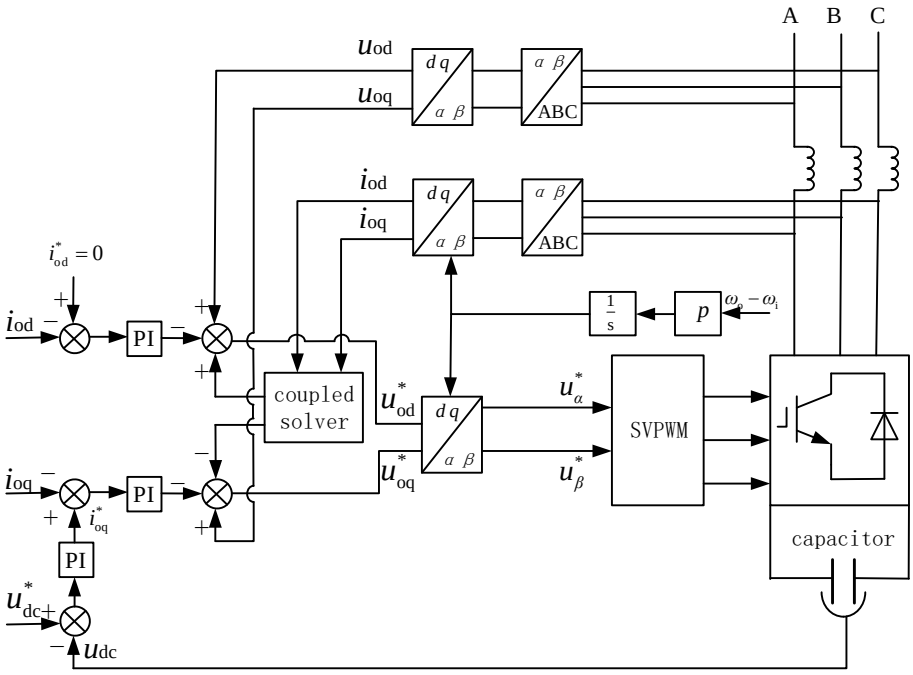


Figure 6. Control block diagram. Notes: ABC is the three-phase winding of the outer rotor, i_{od}*, i_{oq}* are the expected value of dq component of current, u_{od}*, u_{oq}* are the expected value of dq component of voltage, u_{dc} is output voltage of dc side.

4.1. PMSM Based BERS

A conventional PMSM-based BERS, as shown in Figure 2a, serves as the power system for an electric vehicle. When the vehicle slows down, the PMSM can recover part of the braking energy. Figure 7 simulates the energy conversion process of the PMSM-based BERS when the vehicle slows down to 49 km/h at an initial speed of 80 km/h. At the beginning of deceleration, the wheel speed is 671.5 rpm (PMSM is spinning at 2686 rpm). At this moment, the driver decides to slow down the vehicle at rated torque. After 5.42 s, the wheel speed decreases to 412.5 rpm. Due to the PMSM rated speed being 1750 rpm, it works in the constant power zone when the speed is higher than 1750 rpm, as shown in Figure 7a. During this process, the SOC increased from 70% to 71.03%, and the battery open-circuit voltage from 113.605 V to 113.658 V. The controller dealt with 28.26 kJ energy which is stored in the battery.

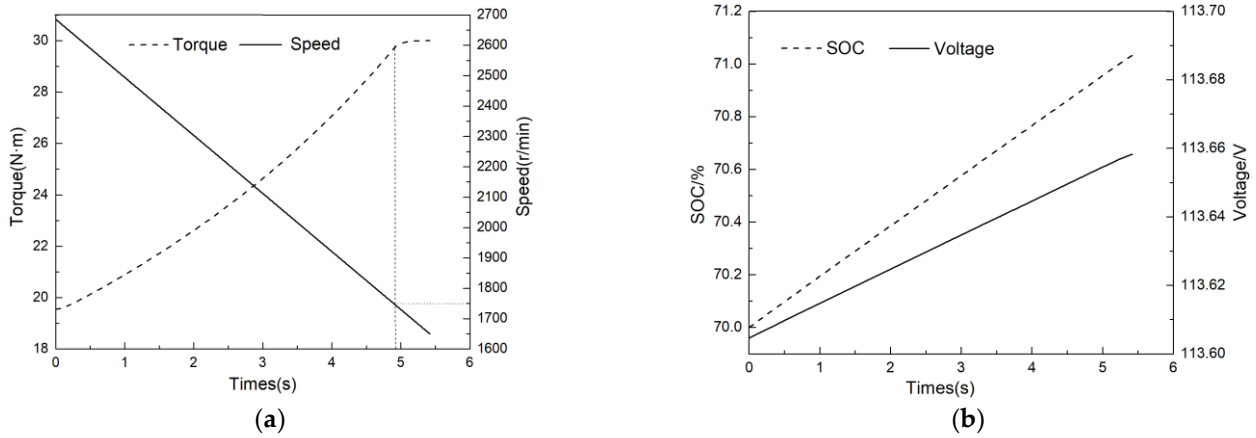


Figure 7. Scenario one simulation results: (**a**) PMSM rotor speed curve; (**b**) SOC curve of battery.

4.2. EC-BERS

In this scenario, the conventional PMSM-based BERS is replaced by the proposed EC-BERS. For the EC-BERS, Figure 8 simulates the energy conversion process of the system when the vehicle is cruising at an initial speed of 80 km/h and decelerating to 49 km/h.

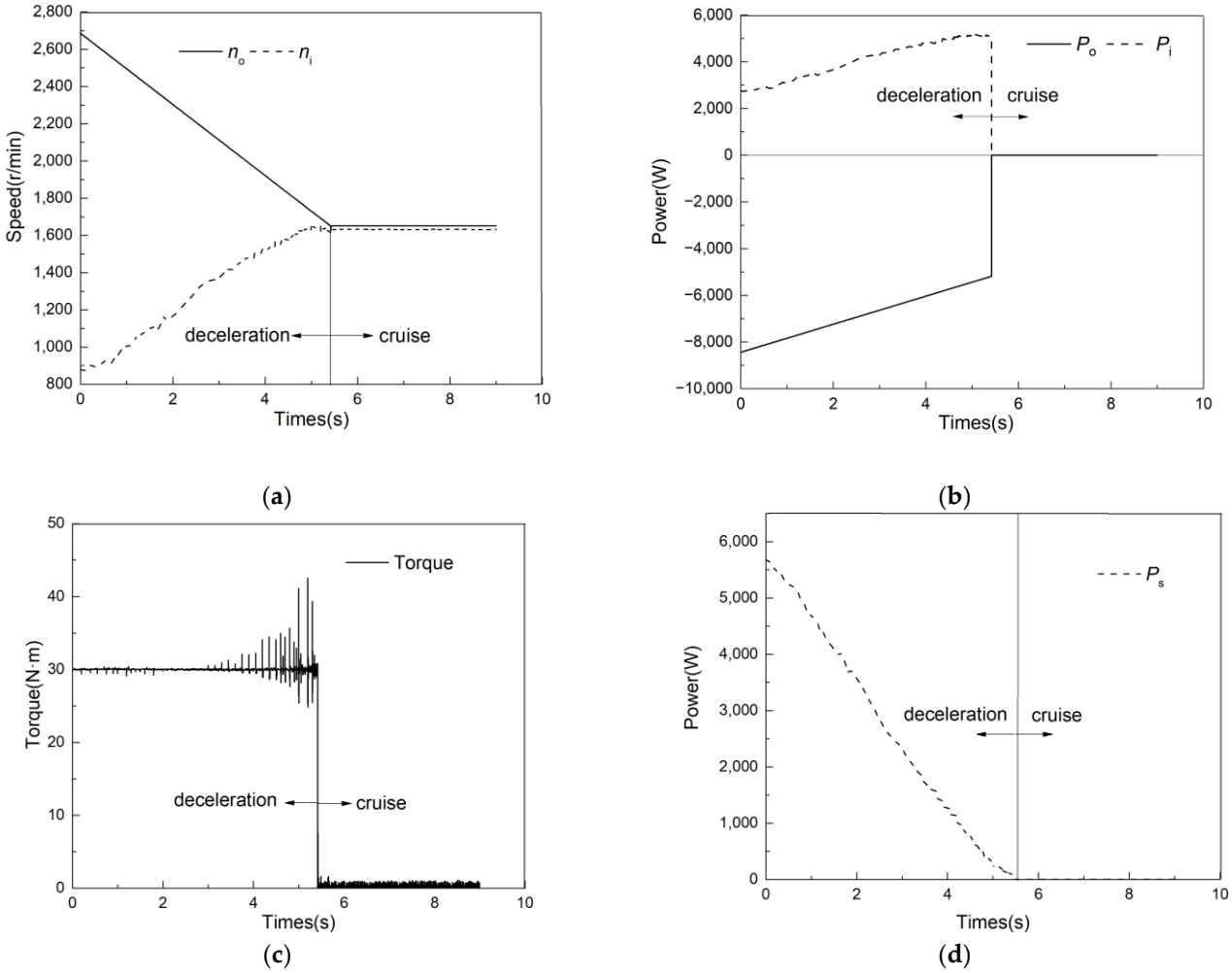


Figure 8. Scenario two simulation results: (**a**) mechanical port speed; (**b**) mechanical port power; (**c**) mechanical port torque; (**d**) electrical port.

As shown in Figure 8a, the initial outer rotor speed is 2686 rpm, which means that the vehicle is cruising at 80 km/h. The inner rotor speed is 879 rpm, which means that the flywheel speed is 4395 rpm. At this moment, −30 N·m is applied to the electromagnetic coupler, and the vehicle speed reaches 49 km/h within 5.42 s. The final flywheel speed increases from 4395 rpm to 8080 rpm. With consideration to Figures 7a and 8c, a conclusion could be found here that the working point of the EC-BERS changes and moves to the high-speed zone compared with the PMSM-based BERS. This phenomenon happens because the PMSM, which is operating at high speeds, cannot provide maximum torque in real time. The electromagnetic coupling braking energy recovery system can give full play to the maximum torque under different speed ranges.

According to Figure 8b, the power absorbed by the flywheel starts from 2.76 to 5.13 kW. Meanwhile, the absorbed power from the vehicle is changing from −8.44 to −5.18 kW. The electrical port power from the electromagnetic coupler changes from 5.67 to 0.11 kW during a deceleration of 0 to 5.42 s, so we can draw an interesting conclusion that the power dealt with by the electrical port is smaller than that of the mechanical port (outer rotor). As a result, about 75.54 kJ energy absorbed from the vehicle is stored in the flywheel, which is

about 2.67 times of the recovered energy in the battery in the PMSM-BERS. Table 3 evaluates two typical scenarios by setting same parameters. For EC-BERS, only 15.53 kJ needs to be dealt with by the electrical port, which is about 0.549 times that of the PMSM-based BERS, and the maximum power transferred by the mechanical port is 8.44 kW. According to Equation (4), i is 0.688. On the basis of satisfying the strengths of the rotors and bearings, the higher the initial deceleration speed, the greater this power, that is, the greater is i.

Table 3. Results for two typical scenarios.

	PMSM-Based BERS	EC-BERS	Changes
Times (s)	5.42	5.42	0
Power (kW)	5.0	8.44	+3.44
Energy dealt with battery (kJ)	28.26	15.53	−12.73
Energy dealt with flywheel (kJ)	-	75.54	-

Notes: "Power" refers to the power input to PMSM or electromagnetic coupler (P_o) from wheels.

5. Test

5.1. Test Platform

For proof of this concept, the EC-BERS test platform was designed and tested. The test platform is shown in Figure 9, and the parameters of each component are shown in Table 4. In order to describe the implementation process of the test more clearly, an EC-BERS powertrain energy flow was marked in Figure 10.

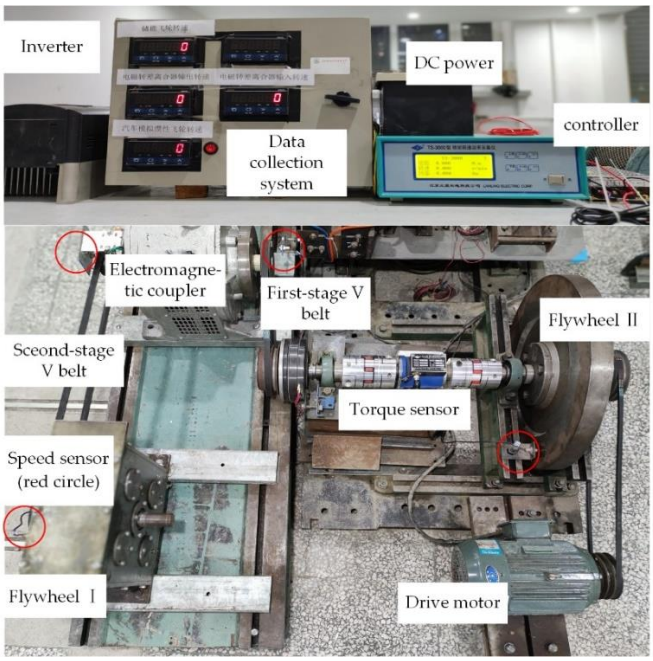


Figure 9. EC-BERS test platform.

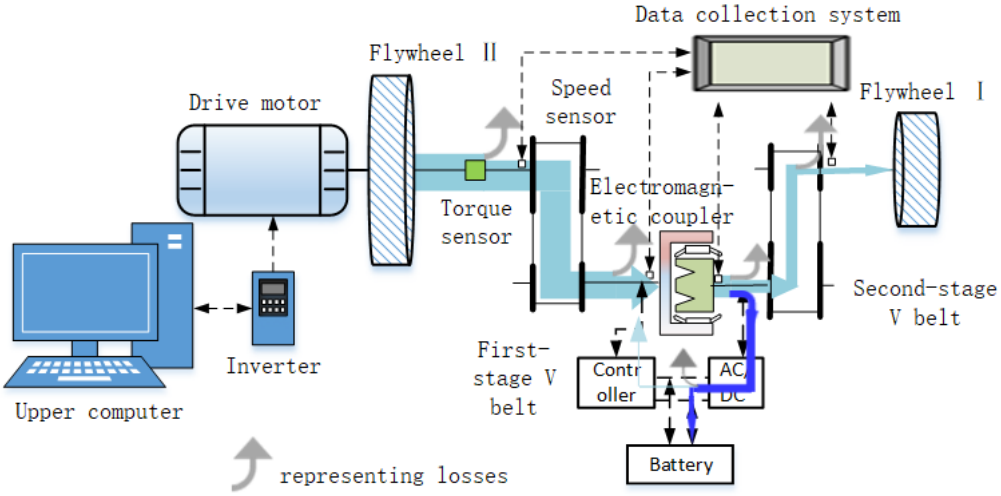


Figure 10. EC-BERS powertrain energy flow (test platform).

This paper adopts the flywheel II to simulate the initial kinetic energy of the vehicle under dynamic conditions. When the flywheel II reaches the specified speed, the PMSM is powered off. At this point, the kinetic energy of flywheel II is the vehicle's kinetic energy when it starts to slow down. Because the V-belt drive can buffer vibration absorption, prevent overload damage of test bench components and is easy to install, the whole test platform adopts the V-belt drive. In order to achieve different initial states for the flywheel II in the test, the inverter is used to control the driving motor, such as acceleration, deceleration, positive rotation, negative rotation and stop. When the flywheel II reaches a specified speed, the drive motor is powered off. The flywheel I directly stores the vehicle's kinetic energy through the first-stage V-belt, the electromagnetic coupler and the second-stage V-belt.

Table 4. Experimental parameters.

Parameters	Unit	Value
Flywheel I inertias	$kg \cdot m^2$	2.99
Flywheel II inertias	$kg \cdot m^2$	4.82
First-stage V belt	-	1:1.20
Second-stage V belt	-	1:1.73
Torque sensor range	Nm	0.1~100
Drive motor rated power	kW	4.0
Drive motor rated speed	$r \cdot min^{-1}$	2890
Drive motor rated torque	N·m	13.2
Electromagnetic coupler rated power/	kW	4.0
Electromagnetic coupler rated speed/	$r \cdot min^{-1}$	1528
Electromagnetic coupler rated torque	N·m	25

5.2. Results Analysis

The initial speed of the flywheel II is 165.6 rad/s (outer rotor angular velocity is 199.2 rad/s) while the flywheel I is 46.9 rad/s (inner rotor angular velocity is 27.1 rad/s), as shown in Figure 11a. At this moment, −25 N·m is applied to the outer rotor until its speed reaches 169.6 rad/s. Meanwhile, the reaction torque rises upward from the inner rotor until it reaches 163.35 rad/s.

Figure 11b,c show the input–output power applied to the electromagnetic coupler mechanical port. The flywheel absorbed power starts from 0.68 kW to 4.09 kW. Meanwhile, the absorbed power from the vehicle is changing from −4.98 kW to −4.24 kW. The electromagnetic coupler's electrical port power changes from 4.31 kW to 0.16 kW during a

deceleration of 0 to 6.4 s. Figure 11c,d present the energy of the electromagnetic coupler and flywheel. From the point of view of energy flow, 28.91 kJ is fed into the electromagnetic coupler, and 15.24 kJ is output as mechanical energy and eventually stored in the flywheel, as seen in Figure 11c. During the process, about 47.3 percent (13.67 kJ) of the initial energy has been temporarily stored in the battery. In theory, all the energy recovered by the PMSM-based BERS goes into the electromagnetic coupler and is stored in the battery, which results in high battery engagement. In fact, the power fed into the outer rotor is determined by the outer rotor speed when the electromagnetic coupler operates at the rated torque. The energy captured by the electrical port is related to the speed difference between the rotors. Therefore, a condition was chosen that could represent the power characteristics of the system during the experiment. Of course, this is not the only case.

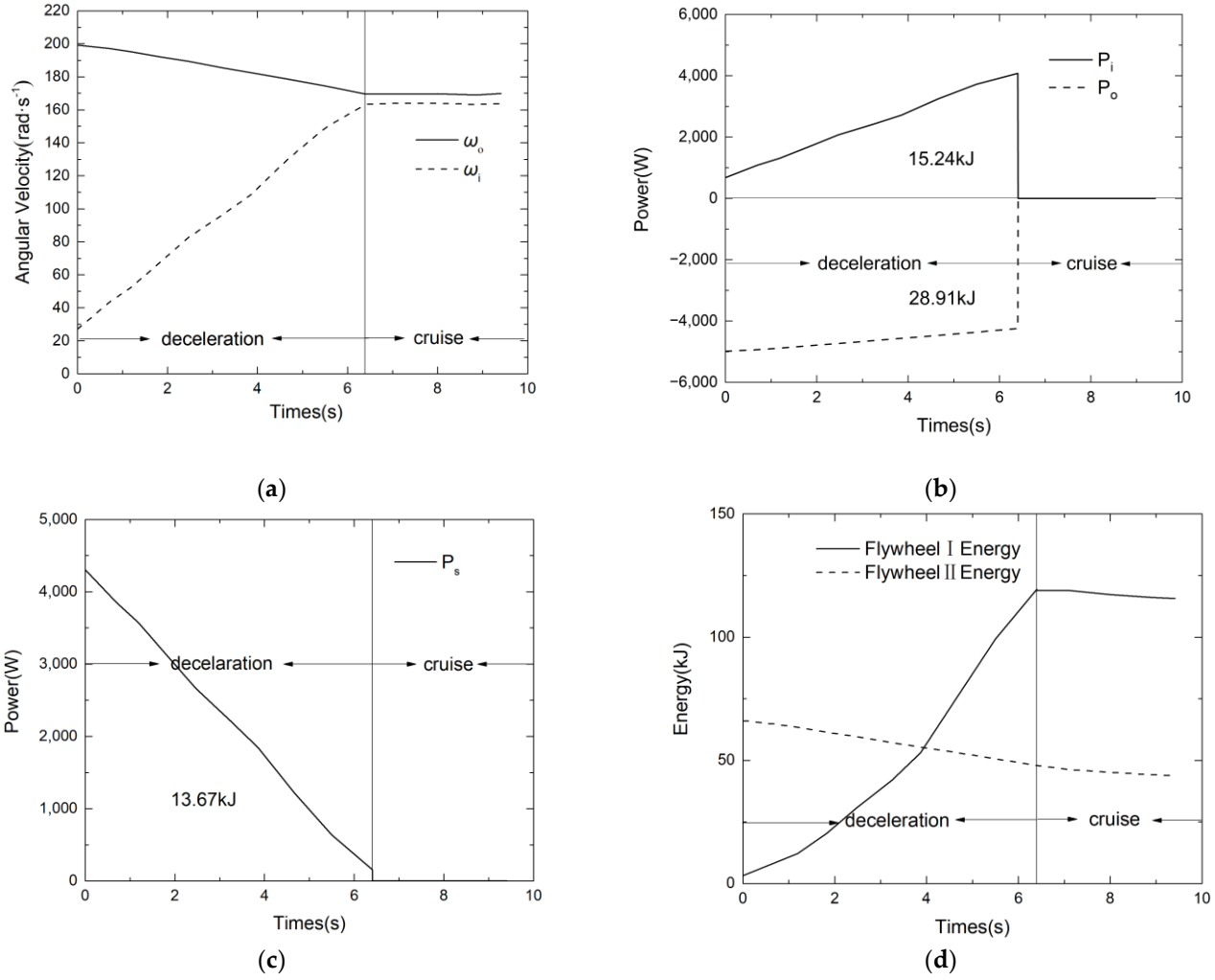


Figure 11. Experimental results: (**a**) mechanical port speed; (**b**) mechanical port power; (**c**) electrical port; (**d**) flywheel energy.

6. Conclusions

Hybrid technology is a method used to improve vehicle efficiency and quality. As an assistant powertrain, the flywheel can meet the peak power requirements of HEV acceleration. During regenerative braking, flywheel systems can not only absorb high power, but can also be much more efficient than batteries. In this paper, the EC-BERS powertrain was introduced to reduce battery engagement, for which the operating principles were described in detail and a mathematical model was presented. In order to represent the characteristics of the EC-BERS more directly, a mathematical model of the PMSM-based BERS was also established. In the same deceleration–cruise conditions, two typical systems

were compared. The results showed that the EC-BERS provided a bidirectional path for mechanical energy transfer between the flywheel and the vehicle. Only the slip energy needed to be dealt with in electrical form, which reduced the battery participation. Furthermore, the proposed system can give full play to the maximum torque under different speed ranges, especially in the high-speed zone. At last, a test platform was designed and tested to verify this concept.

In addition to the above research conclusions, there are some necessary issues that need to be further studied. For example, the gyroscopic effect occurs when the spin axis of a rapidly rotating object changes direction in space. In the proposed EC-BERS system, the rotation axis of the flywheel is along the longitudinal direction of the car body. When the direction of the car movement changes, the gyroscopic effect will appear. To eliminate this effect, a vehicle could be fitted with two flywheels with parallel axes that turn in opposite directions, just as a plane has a double helix that rotates at equal and opposite angular speeds. The gyroscopic effect on the plane's motion would cancel each other out. Furthermore, the flywheel bearing will still be subjected to gyroscopic pressure, which is also a consideration for the future. The flywheel hybrid system is applied to cars as an auxiliary power source and its goal is to ensure that the vehicle has excellent fuel economy. However, the additional mass of the flywheel system conflicts with the goal of achieving lightweight vehicles. How to reasonably control the quality, cost, efficiency, power density and energy density of the flywheel hybrid powertrain to achieve the optimal cost performance under different goals still needs further study.

Author Contributions: Methodology, H.L. and J.C.; software, H.L.; validation, H.L. and S.S.; writing—original draft preparation, H.L.; writing—review and editing, H.L. and J.C. All authors have read and agreed to the published version of the manuscript.

Funding: This research was funded by the National Key Research and Development Program Project of China (Grant No. 2018YFE0207800-04) and the Fundamental Research Funds for the Central Universities of China (Grant No. 2572021DT79).

Institutional Review Board Statement: Not applicable.

Informed Consent Statement: Not applicable.

Data Availability Statement: The data presented in this study are available on request from the corresponding author.

Conflicts of Interest: The authors declare no conflict of interest.

Abbreviations

u_{oq}, u_{od}	outer rotor qd components of voltage
ψ_{oq}, ψ_{od}	outer rotor qd components of flux
R_r	outer rotor resistance
i_{oq}, i_{od}	outer rotor qd components of current
i_f	inner rotor excitation current
L_m	mutual inductance between inner and out rotor
L_{oq}, L_{od}	outer rotor qd components of self-inductance
ω_o, ω_i	angular velocity outer and inner rotor
p	number of pole pairs
T_e	electromagnetic torque
T_{ei}, T_{eo}	electromagnetic torque of inner and outer rotor
T_{mi}, T_{mo}	mechanical torque of inner and outer rotor
B_i, B_o	friction of inner and outer rotor
J_i, J_o	inertia of inner and outer rotor
P_i, P_o	power of inner and outer rotor

References

1. Scharf, C.A. The Crazy Scale of Human Carbon Emission. Available online: https://blogs.scientificamerican.com/life-unbounded/the-crazy-scale-of-human-carbon-emission/ (accessed on 26 April 2017).
2. Concordia University. CO_2 Emissions Cause Lost Labor Productivity. Available online: https://www.sciencedaily.com/releases/2019/10/191011131856.htm (accessed on 11 October 2019).
3. IPPC Sixth Assessment Report. Climate Change 2021: The Physical Science Basis. Available online: https://www.ipcc.ch/report/ar6/wg1/ (accessed on 9 August 2021).
4. British Petroleum (BP). Statistical Review of World Energy. 2020. Available online: https://www.bp.com/en/global/corporate/energy-economics/statistical-review-of-world-energy.html (accessed on 26 October 2021).
5. Zhang, Y.; Chao, Q.; Chen, Y.; Zhang, J.; Wang, M.; Zhang, Y.; Yu, X. China's Carbon Neutrality: Leading Global Climate Governance and Green Transformation. *Chin. J. Urban Environ. Stud.* **2021**, *9*, 2150019. [CrossRef]
6. Chen, H.S.; Liu, C.; Xu, Y.J.; Yue, F.; Liu, W.; Yu, Z.H. The strategic position and role of energy storage under the goal of carbon peak and carbon neutrality. *Energy Storage Sci. Technol.* **2021**, *10*, 1477–1485. [CrossRef]
7. Automotive Industry In-Depth Report 2021: Analysis of Investment Opportunities in the Automotive Industry in the Context of Carbon Neutrality. Available online: https://www.docin.com/p-2657760630.html (accessed on 30 March 2021).
8. China SAE. *Energy Saving and New Energy Vehicle Technology Roadmap 2.0*; China SAE: Beijing, China, 2020.
9. Changzhou Haike New Energy. *Core Technology*; Changzhou Haike New Energy: Changzhou, China, 2012. Available online: http://www.chk-net.com/en/product.asp?id=12 (accessed on 25 November 2020).
10. De Oliveira, J.G. Power Control Systems in a Flywheel Based All-Electric Driveline. Ph.D. Thesis, Uppsala University, Uppsala, Sweden, 2011.
11. Hedlund, M.; Lundin, J.; De Santiago, J.; Abrahamsson, J.; Bernhoff, H. Flywheel Energy Storage for Automotive Applications. *Energies* **2015**, *8*, 10636–10663. [CrossRef]
12. de Oliveira, J.G.; Schettino, H.; Gama, V.; Carvalho, R.; Bernhoff, H. Study on a doubly-fed flywheel machine-based driveline with an AC/DC/AC converter. *IET Electr. Syst. Transp.* **2012**, *2*, 51–57. [CrossRef]
13. Itani, K.; De Bernardinis, A.; Khatir, Z.; Jammal, A. Comparative analysis of two hybrid energy storage systems used in a two front wheel driven electric vehicle during extreme start-up and regenerative braking operations. *Energy Convers. Manag.* **2017**, *144*, 69–87. [CrossRef]
14. Dhand, A.; Pullen, K. Review of flywheel based internal combustion engine hybrid vehicles. *Int. J. Automot. Technol.* **2013**, *14*, 797–804. [CrossRef]
15. Atienza, A.H.; Carino, A.; Jacinto, N. Mechanical Interface of Flywheel Kinetic Energy Recovery System on Motorized Tricycles. *J. Phys. Conf. Ser.* **2020**, *1519*, 012001. [CrossRef]
16. Jingang, G.; Dong, H.; Sheng, W.; Chao, T. Optimum control strategy of regenerative braking energy for electric vehicle. *J. Jiangsu Univ. (Nat. Sci. Ed.)* **2018**, *39*, 132–138.
17. Ehsani, M.; Gao, Y.; Longo, S.; Ebrahimi, K.M. *Modern Electric, Hybrid Electric, and Fuel Cell Vehicles*; CRC Press: Boca Raton, FL, USA, 2018.
18. Mutoh, N.; Nakano, Y. Dynamics of Front-and-Rear-Wheel Independent-Drive-Type Electric Vehicles at the Time of Failure. *IEEE Trans. Ind. Electron.* **2012**, *59*, 1488–1499. [CrossRef]
19. Wu, J.; Xu, Z.; Zhang, F.; Tong, N. Electromagnetic design of high-speed permanent magnet synchronous motor for flywheel energy storage system. *J. Phys. Conf. Ser.* **2021**, *1887*, 012044. [CrossRef]
20. Dougal, R.A.; Liu, S.; White, R.E. Power and life extension of battery-ultracapacitor hybrids. *IEEE Trans. Compon. Packag. Technol.* **2002**, *25*, 120–131. [CrossRef]
21. Rajagopal, S.; Vallikkattil, R.P.; Ibrahim, M.M.; Velev, D.G. Electrode Materials for Supercapacitors in Hybrid Electric Vehicles: Challenges and Current Progress. *Condens. Matter* **2022**, *7*, 6. [CrossRef]
22. Ortuzar, M.; Moreno, J.; Dixon, J. Ultracapacitor-Based Auxiliary Energy System for an Electric Vehicle: Implementation and Evaluation. *IEEE Trans. Ind. Electron.* **2007**, *54*, 2147–2156. [CrossRef]
23. Hansen, J.G.R.; O'kain, D.U. *An Assessment of Flywheel High Power Energy Storage Technology for Hybrid Vehicles*; Oak Ridge National Laboratory: Oak Ridge, TN, USA, 2012. Available online: https://info.ornl.gov/sites/publications/Files/Pub31707.pdf (accessed on 10 June 2021).
24. Pullen, K.R.; Ellis, C.W.H. Kinetic energy storage for vehicles. In Proceedings of the IET—The Institution of Engineering and Technolgy Hybrid Vehicle Conference, Coventry, UK, 12–13 December 2006; pp. 91–108.
25. Ehsani, M.; Singh, K.V.; Bansal, H.O.; Mehrjardi, R.T. State of the Art and Trends in Electric and Hybrid Electric Vehicles. *Proc. IEEE* **2021**, *109*, 967–984. [CrossRef]
26. Chabchoub, M.H.; Trabelsi, H. Improving the efficiency of the energy source of electric vehicles. In Proceedings of the 2020 17th International Multi-Conference on Systems, Signals & Devices (SSD), Sfax, Tunisia, 20–23 July 2020; pp. 410–416. [CrossRef]
27. Ahin, M.E.; Blaabjerg, F.; Sangwongwanich, A. A Comprehensive Review on Supercapacitor Applications and Developments. *Energies* **2022**, *15*, 674. [CrossRef]
28. Rufer, A. The Dream of Efficient Energy Storage-From BESS, KERS & Co. to the Hybrid Power Plant. In Proceedings of the 19th European Conference on Power Electronics and Applications (EPE'17 ECCE Europe), Warsaw, Poland, 11–14 September 2017. [CrossRef]

29. Guney, M.S.; Tepe, Y. Classification and assessment of energy storage systems. *Renew. Sustain. Energy Rev.* **2017**, *75*, 1187–1197. [CrossRef]
30. Hadjipaschalis, I.; Poullikkas, A.; Efthimiou, V. Overview of current and future energy storage technologies for electric power applications. *Renew. Sustain. Energy Rev.* **2009**, *13*, 1513–1522. [CrossRef]
31. Vazquez, S.; Lukic, S.M.; Galvan, E.; Franquelo, L.G.; Carrasco, J.M. Energy Storage Systems for Transport and Grid Applications. *IEEE Trans. Ind. Electron.* **2010**, *57*, 3881–3895. [CrossRef]
32. Tang, T.H. *Fundamentals of Motor and Drive*; China Machine Press: Beijing, China, 2016.
33. Cai, H.; Xu, L. Modeling and Control for Cage Rotor Dual Mechanical Port Electric Machine–Part I: Model Development. *IEEE Trans. Energy Convers.* **2015**, *30*, 957–965. [CrossRef]
34. Ershad, N.F.; Mehrjardi, R.T.; Ehsani, M. Efficient Flywheel-Based All-Wheel-Drive Electric Powertrain. *IEEE Trans. Ind. Electron.* **2021**, *68*, 5661–5671. [CrossRef]
35. Xia, L.; Jiang, H.B. Design and Steady-State Performance of a Novel Winding Type Permanent Magnet Coupling with Slip Power Recovery Function. *Math. Probl. Eng.* **2017**, *2017*, 3141089. [CrossRef]
36. Nasiri, H.; Radan, A.; Ghayebloo, A.; Ahi, K. Dynamic modeling and simulation of transmotor based series-parallel HEV applied to Toyota Prius 2004. In Proceedings of the 10th International Conference on Environment and Electrical Engineering, Rome, Italy, 8–11 May 2011. [CrossRef]
37. Jiang, H.B.; Tang, B.; Xu, Z.; Geng, G.-Q. Electromagnetic and Torque Characteristics of Electromagnetic Slip Coupling Applied to Hydraulic Power Steering System for Heavy-Duty Vehicles. *J. Comput. Theor. Nanosci.* **2015**, *12*, 1069–1075. [CrossRef]